

# Power Optimization of Ultrasonic Friction-Modulation Tactile Interfaces

Michaël Wiertlewski and J. Edward Colgate, *Fellow, IEEE*

**Abstract**—Ultrasonic friction-modulation devices provide rich tactile sensation on flat surfaces and have the potential to restore tangibility to touchscreens. To date, their adoption into consumer electronics has been in part limited by relatively high power consumption, incompatible with the requirements of battery-powered devices. This article introduces a method that optimizes the energy efficiency and performance of this class of devices. It considers optimal energy transfer to the impedance provided by the finger interacting with the surface. Constitutive equations are determined from the mode shape of the interface and the piezoelectric coupling of the actuator. The optimization procedure employs a lumped parameter model to simplify the treatment of the problem. Examples and an experimental study show the evolution of the optimal design as a function of the impedance of the finger.

**Index Terms**—Ultrasonic, surface haptics, haptics, tactile interface, variable friction.

## 1 INTRODUCTION

IN the recent years, human-computer interaction has become increasingly dominated by touch screens. Despite the obvious benefit of the co-localization of visual information and touch input, this change has rendered the interface tactually poor. Users are confronted with a flat panel with no apparent tactile features to guide their finger movements. As a result, considerable effort has been expended in order to bring tangibility to touch screens. The most common approach makes use of the high sensitivity of human touch to transients by vibrating the entire device with complex waveforms. Electromagnetic or piezoelectric actuators are placed in the device and send vibratory signals through the case in contact with the user's skin. The range of frequencies provided falls into a bandwidth compatible with tactile perception (i.e. 20 to 800 Hz) [1], [2], [3], [4]. Focalization of waves using time-reversed acoustics has been used to localize the vibration with remote actuators [5], [6]. Another direction makes use of electrostatic interaction to modulate the friction force experienced by a finger exploring the screen [7], [8], [9].

### 1.1 Friction reduction via transverse ultrasonic waves

This article explores the design of a class of devices that use ultrasonic transverse vibration to reduce the friction between a plate and the fingertip. This effect was pioneered by Watanabe et Fukui [10]. They used

Langevin transducers to create a transverse standing wave on a steel plate covered with sandpaper. They noted that the perceived roughness of the sandpaper decreased with increasing amplitude of the vibration. Since then, efforts have been made to use this effect for rendering complex tactile stimuli directly to the fingertip. Biet et al. proposed a design based on a Beryllium-Copper plate with piezoelectric actuators bonded to one side [11]. The assembly creates a monomorph that deforms into a sinusoidal standing wave, generating the reduction of friction over the entire surface of the plate. Winfield et al. used a circular glass substrate bonded to a piezoelectric actuator to create a drum-type standing wave [12]. While these designs were opaque, more recent designs have localized the piezoelectric actuators at the edge of a transparent glass plate where they excite a standing wave, owing to the propagation of bending waves. The actuators are either glued directly onto the glass plate [13] or by using a composite actuator bonded to the side of the plate [14].

### 1.2 Design process

Ultrasonic friction reduction devices are built around the resonance of a plate to achieve a large enough displacement amplitude at ultrasonic frequencies, typically 1  $\mu\text{m}$  at 35 kHz. After choosing the mode shape [13], [15] and the frequency at which the device will be operated, the main concern is often to increase the efficiency of the device and consequently to reduce the amount of energy provided to the piezoelectric actuator. Efficiency is a critical figure for embedded and battery powered devices. Giraud et al. [16] argued that the main factor for energy losses comes from the dielectric losses in the actuator and that, in order to minimize the losses, the actuators should be as thin

• M. Wiertlewski and J.E. Colgate are with the Department of Mechanical Engineering, Northwestern University, Evanston, IL, 60208-3111, USA.

E-mail: {wiertlewski,colgate}@northwestern.edu

as possible. While this reasoning is perfectly valid for a plate without any loading, the same analysis cannot be achieved if we consider that the actuator must provide a minimum amount of power to deform the skin. An optimum thickness of the piezoelectric actuator and the supporting medium must exist as thick devices bear large losses due to the increased volume of material while thin devices may not be powerful enough to deform the finger.

In certain cases, such as high-fidelity haptics, the efficiency is a secondary factor in the design procedure with respect to the ability to render complex frictional waveforms. Rendering high-frequency content via a friction reduction device, is achieved by the rapid modulation of the amplitude of the standing wave. The carrier frequency is modulated with a lower frequency waveform representing the tactile signal, typically in the range of dc to 500 Hz. The system is resonant and the changes in oscillation amplitude come with a rise time that depends of the quality factor of the plate. For a high quality factor (typically 150), the rise time can reach 10 ms, limiting the bandwidth to frequencies below 100 Hz. Designing around the resonant properties of the plate creates a tradeoff between maximum amplification of the motion and the rapidity of the amplitude modulation [17], [18].

The method presented in this article synthesizes the motion of the plate and the actuators into a lumped-parameter model. Plate dynamics and the actuator electromechanical transformation are modeled as lumped elements around the working frequency using a Lagrange formulation. With the help of this model, the efficiency and the quality factor of the system are derived and optimized with respect to the load impedance that the fingertip provides. Optimization shows that there exists an impedance of the device that maximizes power efficiency.

## 2 DEVICE DESIGN

### 2.1 Principle of operation

The scope of this article covers the design of a rectangular plate excited with a  $n \times 0$  standing wave<sup>1</sup>, which is a robust way for providing friction reduction with the maximum uniformity of the effect compared to  $n \times m$  mode shape [13]. In this mode, the nodal lines are straight, parallel to one edge of the plate, and equally spaced. The actuators are bonded to one end of the plate in alignment with the nodal lines. The shape of the actuator influences the modes that are excited [19]. Using a rectangular piezoelectric actuator a half-wavelength wide and as long as the edge of the plate enforces the  $n \times 0$  mode shape, providing optimal friction reduction. An illustration of this geometry is shown in Fig. 1a.

1. Notably, this does not include square plates, which, due to their symmetry, tend to exhibit  $n \times n$  mode shapes in preference to  $n \times 0$ .

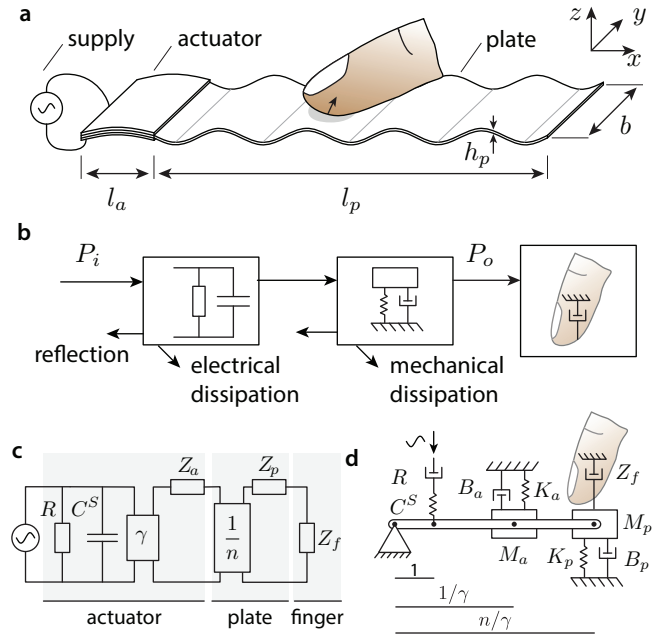


Fig. 1. **a.** Typical friction reduction device. **b.** Power transformation diagram. The input power  $P_i$  is transformed and carried to the finger where only a fraction  $P_o$  remains. Reflection and dissipation of energy reduce the device efficiency. **c.** Electrical representation of the lumped-parameter model of the device. **d.** Mechanical analog.

The power is delivered to the finger through a series of intermediate elements. First, the electrical power is sent to the piezoelectric actuator. Part of the energy is stored in the internal capacitance of the actuator and may be reflected if one uses an inductance to recycle this energy. A fraction of the energy is converted into mechanical energy that is employed to deform the actuator, the plate, and finally the finger. Dissipation also occurs in the surrounding air. The flow of power is depicted in Fig. 1b.

In order to provide the reader with typical values used during the design of ultrasonic friction reduction devices, this article presents numerical values for each parameter via a representative device that has a workspace of 120x90 mm on a 1 mm thick borosilicate glass. These dimensions are chosen to fit a 4 inch display. For this configuration, the model described in section 3 through 6 of this article predicts an efficiency of 73% and a total peak power of 1.3 W. The properties of the materials used for the simulation and the experiments are reported in table 1. The notation follows the IEEE Standard on Piezoelectricity as closely as possible.

### 2.2 Lumped-parameter model

A lumped-parameter approach reduces the complexity of the model to simple elements that are dependent on the material properties and the geometrical

dimensions of the assembly. The model captures the electrical and mechanical behavior of the actuator, the vibration of the plate, and the impedance provided by the finger. Electrical and mechanical representations of the simplified model can be found in Fig.1c and Fig.1d respectively. This article is organized by examining the contribution of each element, starting from the end and working our way back to the power supply. Once the value of each element is derived as a function of external dimensions, the optimization procedure is explained.

It is worth taking into consideration that the lumped-parameter model is valid only around the resonant frequency at which the normal mode is excited. The model also assumes that the connection between the actuator and the plate coincides with a nodal line.

### 3 TERMINAL IMPEDANCE

The acoustic energy of the plate is dissipated in two ways: into the finger, and into the surrounding fluid (i.e. air). The plate's energy can also be dissipated via the mounting structure into the remainder of the device, but these losses can be minimized by mounting along nodal lines and are ignored here. The mounting device can also radiate acoustic energy and be a substantial source of energy losses. To minimize the damping provided by the frame, it is usual practice to attach the plate with compliant material at the location of nodal lines.

#### 3.1 Dissipation via the fingertip

The fingertip, touching the vibrating glass plate, experiences a reduction of the friction resisting its lateral motion. This effect is likely to be caused by a combination of both air trapping under the contact area and intermittent contact due to the disconnection of the plate and the skin. In an attempt to simplify the expression for the losses due to the finger touching the surface, we consider that the finger is always in contact with the plate and that acoustic energy is radiated inside the tissues. We make the assumption that the contact between the finger is a single point at an anti-node of the plate. In order to provide the reader with a illustrative value of the impedance, the fingertips is modeled as an infinite vertical beam made from elastic material. The motion of the plate uniformly compresses the beam, propagating acoustic energy into the tissues. The stratum corneum has a Young's modulus as high as  $Y_s = 5$  MPa [20] and usually the same density as water, i.e.  $\rho = 1000$  kg/m<sup>3</sup>. The area of contact of the fingertip is approximately  $S = 180$  mm<sup>2</sup> under light touch [21]. Considering those values, the driving point impedance of the finger according to the compressed beam model is  $Z_f = S \cdot \sqrt{Y_s \rho} \approx 12$  N.s/m. The experimental characterization presented in section 7.3.3 of this article

shows that the impedance of the finger is closer to 20 N.s/m for a light touch. The higher value is likely to be attributed to the viscoelasticity of the tissues. The power drawn by the finger when harmonically stimulated with an amplitude of  $u_p = 1$   $\mu$ m and a frequency of  $f = 35$  kHz is  $P = Z_f (2\pi f u_p)^2 = 960$  mW. We emphasize that the power transmitted to the finger will also depend on the position of the contact with the plate. Because the plate deforms in a sinusoidal pattern with a wavelength on the same order of magnitude as the contact diameter of the fingertip, the transverse deformation of the skin is not uniform. It will be maximum when the center of pressure is touching an anti-node and minimum when touching a nodal line.

#### 3.2 Acoustic radiation into the air

The transverse vibrations of the plate induce a displacement field in the surrounding fluid that can propagate outward thus radiating energy [22]. The critical parameter in the determination of losses is the ratio between the speed of sound in air and the speed of the bending waves in the plate. If the speed of the bending wave is supersonic, losses may be approximated by the radiation of a single piston of the same area as the plate. Conversely, if the speed of the bending wave remains below the supersonic threshold, the air acts like an added mass and losses are much reduced. In a rectangular plate, bending wave propagation speed is given by  $\sqrt{\omega h} \cdot \left(\frac{Y}{12\rho}\right)^{\frac{1}{4}}$ , with  $Y$  the Young's modulus and  $\rho$  the density of the medium. Considering a speed of sound in air of 340 m/s, this critical speed translates into a thickness of borosilicate glass of  $h = 0.3$  mm when excited at  $\omega/2\pi = 35$  kHz. If the thickness is lower than the critical thickness the radiated energy is several order of magnitude lower than the losses due to the material. In the worst case, losses are computed by taking the average velocity across the plate as the equivalent piston velocity:

$$P_{air} = \frac{1}{2} \rho_{air} c_{air} \int_S \dot{\mathbf{u}}^2 dS \quad (1)$$

where  $\rho_{air}$  is the density of the air,  $c_{air}$  is the speed of sound in air,  $S$  is the radiating surface and  $\mathbf{u}(x, y)$  is the peak amplitude of motion at the position  $x, y$ . For the reference design described in 2.1 excited at 35 kHz and having a sinusoidal mode shape of amplitude 1  $\mu$ m, the losses amount to 120 mW.

### 4 FREE VIBRATION OF THE PLATE

The resonating plate has a length  $l$  and width  $b$ . The mode shape associated with the resonance of the plate depends on both boundary conditions and the actual length. The placement of the piezoelectric actuator is optimal when it fills one full region between nodal

lines. In that case the boundary may be treated as simply supported. At the other end of the plate, the boundary condition is specified by the designer. Knowing the boundary conditions, the mode shape can be easily derived [23]. For instance, a simply supported plate, excited in a  $n \times 0$  normal mode will have a displacement  $\mathbf{u}_p(x, y, t) = u_p(t) \cdot \sin(\beta_p x)$ , with  $\beta_p = \frac{2\pi}{\lambda_p} = \frac{n\pi}{l}$  the wavenumber,  $\lambda_p$  the wavelength,  $n = \{1, 2, 3, \dots\}$  the number of nodal points and  $u_p(t)$  the instantaneous amplitude.

#### 4.1 Energy stored in the plate

The equation of motion is retrieved from inspection of the kinetic and potential energy. The kinetic energy is:

$$\mathcal{T}_p = \int_V \frac{1}{2} \rho_g \dot{\mathbf{u}}_p^2 dV = \frac{1}{2} M_p \dot{u}_p^2(t) \quad (2)$$

where  $\rho_g$  is the glass density,  $V$  the plate volume and  $M_p = \rho_g b h_p \frac{l_p}{2}$  is the equivalent mass of the vibrating plate. The expression for the potential energy, based on Euler-Bernoulli beam theory, is  $\mathcal{V}_p = \int_V \frac{1}{2} Y_g S_{11}^2(x, z) dV$ , where  $Y_g$  is the Young's modulus of glass and  $S_{11}(x, z)$  is the compressive strain along the  $x$  axis at the coordinate  $(x, z)$ . A consequence of Euler-Bernoulli theory is that  $S_{11}(x, z) = -z \frac{\partial^2 u}{\partial x^2}$ . Considering an isotropic material this leads to:

$$\mathcal{V}_p = \frac{1}{2} Y_g b \int_{-h_p/2}^{h_p/2} z^2 dz \int_0^{l_p} \left( \frac{\partial^2 \mathbf{u}_p}{\partial x^2} \right)^2 dx = \frac{1}{2} K_p u_p^2(t) \quad (3)$$

where  $K_p = Y_g \frac{b h_p^3}{12} \frac{l}{2} \beta_p^4$  is the equivalent stiffness.

Under harmonic excitation  $u_p(t) = \bar{u}_p e^{i\omega t}$ , resonance is achieved when the potential energy and the kinetic energy are equal, leading to a condition on the wavenumber:  $\beta_p^4 = \frac{\omega^2}{h_p^2} \frac{12\rho_g}{Y_g}$ . This condition is necessary for resonance to occur. For the reference design,  $M_p = 11$  g and  $K_p = 560$  kN.mm<sup>-1</sup>.

#### 4.2 Internal dissipation

Every material exhibits losses due to inelastic deformation. These losses are captured using a complex valued Young's modulus  $Y_g = Y_g' + iY_g''$  and taking the imaginary part of equation 3. The dissipation can be put into perspective considering that the plate is acting as a damped second-order system around the resonance. The resonant frequency is defined by  $\omega_0 = \sqrt{\frac{K_g}{M_g}}$  and the quality factor is  $Q = \frac{K_p}{\omega_0 B_p}$ , with  $B_p$  the effective damping found using the complex value Young's modulus. The reference design has a  $B_p = 3.6$  N.s.m<sup>-1</sup>. The quality factor, also called Q-factor, is a measure of the energy dissipation with respect to the energy stored in the system. The higher the value of the quality factor, the lower the losses and the larger the amplitude at resonance.

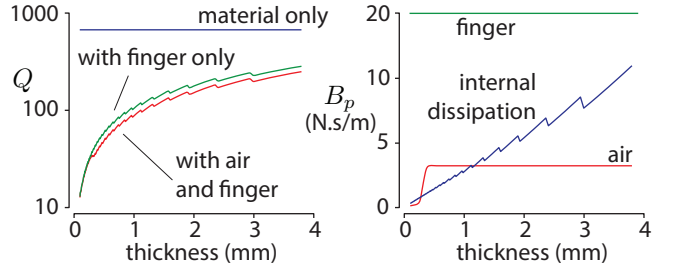


Fig. 2. Plate quality factor and damping elements as a function of thickness.

#### 4.3 Influence of thickness

Figure 2 shows the evolution of dynamic parameters as a function of the thickness for the reference design described in 2.1. First, the actual length is calculated using  $l_p = \frac{\pi}{\beta} \text{round}(\frac{l_m \beta}{\pi})$  then dynamic parameters are found using to the aforementioned equations. Rounding the length causes jumps in the value of parameters as the number of full wavelength increases. The value of the quality factor, damping and admittance are calculated with and without the influence of the finger and surrounding air. In the absence of an external dissipation mechanism, the quality factor remains constant by definition. Thinner glass allows for lower dissipation as the volume of material decreases.

### 5 ELECTROMECHANICAL CONVERSION

#### 5.1 Actuator construction

The actuator consists of two piezoelectric rectangular plates, glued to each side of the glass substrate as shown in Fig. 3. The assembly provides actuation to the rest of the plate by the transmission of acoustic energy. The plate and the actuator section share the same neutral axis.

Typical construction uses an actuator on one side only. The asymmetry of this configuration causes a shift of the neutral axis away from the center changing the formulation of the model. The reader can refer to [15] for guidance on modeling this situation. For the sake of simplicity, single-sided actuators are not

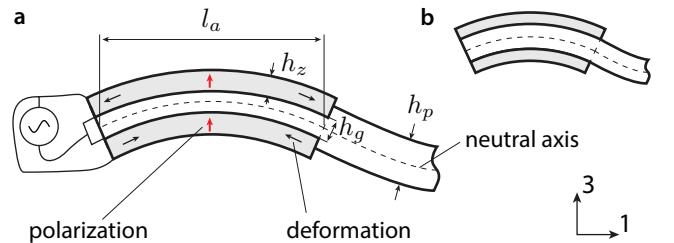


Fig. 3. The actuator is built from the assembly of two piezoelectric plates glued to the glass substrate. **a.** Parametrization of the problem. **b.** Configuration when the piezoelectric actuators are glued directly to the plate and  $h_g = h_p$ .

covered in this article. However, for a piezoelectric plate at least 2 times thinner than the glass substrate, the current model gives a good approximation of the behavior.

## 5.2 Energy Stored in the Actuator

The actuator is also excited by a standing wave of the form  $\mathbf{u}_a(x, y, t) = u_a(t) \cdot s(x)$ , where  $s$  is the mode shape. The mode shape is determined by the boundary conditions of the actuator. A discussion of the influence of the mode shape on the parameters is given in appendix A. The kinetic energy formulation is quite similar to the one for the plate, but is modified to account for the influence of both materials:

$$\mathcal{T}_a = \int_V \frac{1}{2} \rho \dot{\mathbf{u}}_a^2 dV = \frac{1}{2} M_a \dot{u}_a^2(t) \quad (4)$$

with

$$M_a = (\rho_g h_g + \rho_z 2h_z) b \int_0^{l_a} s^2(x) dx \quad (5)$$

where the indices  $g$  and  $z$  stand for the glass and the piezoelectric materials. The piezoelectric effect is reversible. A mechanical action on the crystal produces electrical charges and conversely a voltage applied across the polarization dimension produces a deformation. To capture the phenomenon it is common to write the constitutive equations in the form:

$$\begin{pmatrix} S_1 \\ D_3 \end{pmatrix} = \begin{pmatrix} 1/Y_{11}^E & d_{31} \\ d_{31} & \varepsilon_{33}^T \end{pmatrix} \begin{pmatrix} T_1 \\ E_3 \end{pmatrix} \quad (6)$$

where the indices 1 to 3 represent the axis of the coordinate system relative to the polarization. In this configuration 1,2,3 stand for the  $x, y, z$  axes respectively.  $S_1$  is the strain along  $x$ ,  $D_3$  the current density in the  $z$  direction,  $T_1$  is the stress in the  $x$  direction and  $E_3$  is the electric field strength in the  $z$  direction.  $Y_{11}^E$ ,  $\varepsilon_{33}^T$ ,  $d_{31}$  are the Young's modulus at zero field (short circuit), the permittivity at zero stress (free end) and the piezoelectric strain coefficient, respectively.

To calculate the combined electrical and mechanical potential energy, an expression of the stress as a function of strain is needed. Rearrangement of the first line of equation 6 leads to the transformation:

$$\begin{pmatrix} T_1 \\ D_3 \end{pmatrix} = \begin{pmatrix} Y_{11}^E & -e_{31} \\ e_{31} & \varepsilon_{33}^S \end{pmatrix} \begin{pmatrix} S_1 \\ E_3 \end{pmatrix} \quad (7)$$

where  $\varepsilon_{33}^S = \varepsilon_{33}^T (1 - k_{31}^2)$  is the permittivity at zero strain,  $k_{31} = d_{31} / \varepsilon_{33}^T Y_{11}^E$  is the electromechanical coupling coefficient and  $e_{31} = d_{31} Y_{11}^E$  is the piezoelectric field to strain coefficient. Following the calculation derived by Premont [24], the potential energy stored in the electromechanical system is found to be:

$$\begin{aligned} \mathcal{V}_a &= \int_V \frac{1}{2} Y_{11} S_1^2 - \frac{1}{2} \varepsilon_{33}^S E_3^2 + e_{31} S_1 E_3 dV \\ &= \frac{1}{2} K_a a_a^2(t) + \frac{1}{2} C^S v^2(t) + \gamma u_a(t) v(t) \end{aligned} \quad (8)$$

with

$$\begin{aligned} K_a &= \frac{2}{3} Y_g b \left[ \frac{Y_{11}}{Y_g} \left( \frac{h_g}{2} + h_z \right)^3 \right. \\ &\quad \left. + \left( 1 - \frac{Y_{11}}{Y_g} \right) \left( \frac{h_g}{2} \right)^3 \right] \int_0^{l_a} \left( \frac{d^2 s}{dx^2} \right)^2 dx \end{aligned} \quad (9)$$

the stiffness of actuator. The integration over the thickness accommodates for the composite structure of the bimorph actuator. The capacitance is written as

$$C^S = 2 \varepsilon_{33}^S \frac{bl}{h_z} \quad (10)$$

where the factor 2 is due to the parallel connection of the upper and lower electrodes. Lastly, the piezoelectric coupling factor is:

$$\begin{aligned} \gamma &= \frac{b}{h_z} \left[ \int_{-\frac{h_g}{2}}^{-\frac{h_g}{2} + h_z} -e_{31} z dz + \int_{\frac{h_g}{2}}^{\frac{h_g}{2} + h_z} e_{31} z dz \right] \int_0^{l_a} \frac{d^2 \mathbf{u}_a}{dx^2} dx \\ &= e_{31} b (h_z + h_g) \int_0^{l_a} \frac{d^2 s}{dx^2} dx \end{aligned} \quad (11)$$

The sign of the electromechanical coupling factor in the above formula reflects the parallel configuration of each piezoelectric plate. One plate expands while the other contracts, which in turn produces a bending deformation of the composite structure.

## 5.3 Dissipation mechanisms

The dissipation mechanism in piezoelectric material has been approached in a number of different ways [25], [26], [27]. This article takes into account two mechanisms: mechanical damping and electrical losses. The presence of both dissipation mechanisms in the model provides sufficient realism to find an optimum solution. Damping is found by using the complex Young's modulus in the definition of the material and taking the imaginary part of the stiffness formulation:

$$\begin{aligned} B_a &= \frac{2}{3} Y_g'' b \left[ \frac{Y_{11}''}{Y_g''} \left( \frac{h_g}{2} + h_z \right)^3 \right. \\ &\quad \left. + \left( 1 - \frac{Y_{11}''}{Y_g''} \right) \left( \frac{h_g}{2} \right)^3 \right] \int_0^{l_a} \left( \frac{d^2 s}{dx^2} \right)^2 dx \end{aligned} \quad (12)$$

The dielectric losses are determined with the help of the loss tangent. They are modeled as a resistor in parallel with the actuator's capacitance. This model does not hold for low frequencies and continuous current but is valid around the working ultrasonic frequency. The value of the equivalent parallel resistor is:

$$R = (\omega_r C^S \tan \delta)^{-1} \quad (13)$$

with  $\omega_r / 2\pi$  the frequency at which  $\tan \delta$  is measured, typically 1 kHz. Both values are supplied by the manufacturer. The power dissipated is  $\mathcal{D}_e = \frac{1}{2} \frac{1}{R} v^2(t)$  where  $v$  is the voltage across the actuator electrodes.

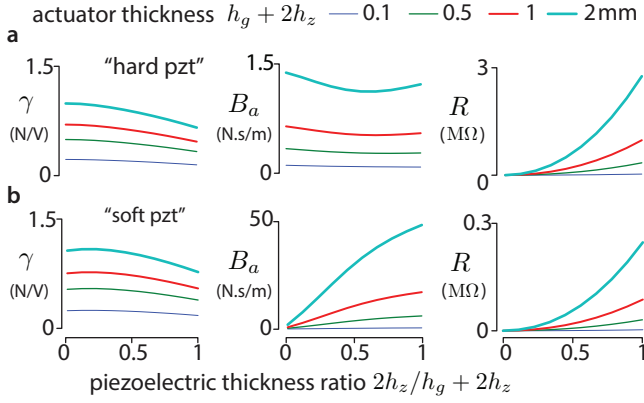


Fig. 4. Actuator conversion factor and losses as a function of the total thickness and the proportion of piezoelectric material. **a.** Simulation using *hard* piezoceramic. **b.** Simulation using *soft* piezoceramic.

Using low losses actuators with thickness of 0.4 mm, the value of the lumped elements for the reference design are  $\gamma = 0.92 \text{ V.N}^{-1}$ ,  $M_a = 4.3 \text{ g}$ ,  $B_a = 1.1 \text{ N.s.m}^{-1}$ ,  $K_a = 209 \text{ kN.mm}^{-1}$ ,  $C^s = 0.4 \text{ nF}$ , and  $R = 0.5 \text{ M}\Omega$ .

#### 5.4 Influence of piezoelectric actuator thickness

The dependence of actuator dynamic parameters upon the relative thickness of both materials is shown in figure 4. These calculations assume that the actuator has pinned-pinned boundary conditions and a single half-wavelength mode shape. As mechanical losses arise mainly from the piezoelectric material, the damping is strongly correlated with its volume. Material properties are summarized in table 1.

TABLE 1  
Material coefficients

		Borosilicate glass	Soft PZT-5A	Hard PZT-4
$Y_{11}^E$	(GPa)	74	51	86
$Q_m$		750	100	1400
$\rho$	$10^3 \text{ (kg/m}^3\text{)}$	2.5	7.8	7.9
$\varepsilon_{33}^T / \varepsilon_0$		-	2500	1350
$k_{31}$		-	0.43	0.40
$\tan \delta$	$(10^{-4} \text{ rad})$	-	200	40
$d_{31}$	$10^{-12} \text{ (m/V)}$	-	190	130

#### 5.5 Amplitude magnification

Because the piezoelectric actuators are glued onto the glass plate, they increase overall thickness, and therefore increase acoustic impedance relative to the rest of the plate. One consequence of this impedance mismatch is that the amplitude of the plate motion will be greater than that of the heavier and stiffer plate-plus-actuator region. Using an argument similar

to that used to model compression wave amplification in step horns [23], the amplification in our case can be found by treating the location of the thickness step as a nodal line. The origin  $x = 0$  is taken at the nodal

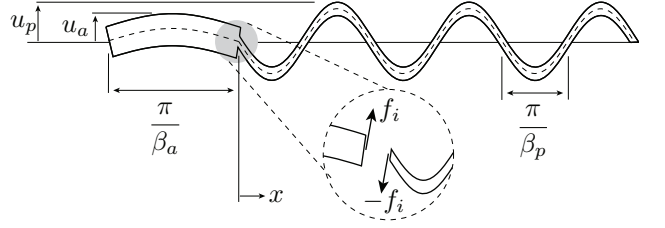


Fig. 5. The motion amplitude is higher for the thinner section. The difference in thickness is captured by an amplification factor  $n$  in the model which is derived from the equilibrium of forces at the interface.

point. In that case, Newton's third law at the junction of the plate and the actuator requires that the force  $f_i$  is equal on either side as depicted in figure 5. This leads to:

$$f_i = Y_g \frac{bh_a^3}{12} \frac{d^3 \mathbf{u}_a}{dx^3} \Big|_{x=0} = Y_g \frac{bh_p^3}{12} \frac{d^3 \mathbf{u}_p}{dx^3} \Big|_{x=0} \quad (14)$$

with  $h'_a = 2 \left( \frac{Y_{11}}{Y_g} \left( \frac{h_g}{2} + h_z \right)^3 + \left( 1 - \frac{Y_{11}}{Y_g} \right) \left( \frac{h_g}{2} \right)^3 \right)^{\frac{1}{3}}$  the thickness of the actuator if it was made of the same material as the plate. Assuming that the motion of the actuator and the plate are sinusoidal  $\mathbf{u}_a = u_a \sin \beta_a x$  and  $\mathbf{u}_p = u_p \sin \beta_p x$ , with  $\beta_a$  and  $\beta_p$  the wavenumber of the actuator and the plate respectively, the previous equation simplifies to:

$$h_a^3 \beta_a^3 u_a = h_p^3 \beta_p^3 u_p \quad (15)$$

The wavenumber for the actuator is  $\beta_a = \sqrt[4]{\omega^2 \frac{12 \rho_a}{Y_g h_a^2}}$  with  $\rho_a h'_a = \rho_g h_g + \rho_z 2h_z$  the equivalent surface density. Remembering that  $\beta_p = \sqrt[4]{\omega^2 \frac{12 \rho_g}{Y_g h_p^2}}$ , we can show that the amplification factor is:

$$n = \frac{u_p}{u_a} = \left( \frac{h'_a}{h_p} \right)^{\frac{3}{2}} \cdot \left( \frac{\rho_a}{\rho_g} \right)^{\frac{3}{4}} \quad (16)$$

This model assumes that the slope of the neutral axis is discontinuous at the junction between the actuator and the glass. While this assumption provides a sufficiently good representation of the amplification factor, as the experimental validation will show later in the article, the behavior at the thickness step might be better described by Timoshenko beam theory or finite element analysis. This model is a particular case where the connection between the two sections happens to coincide with a nodal line. For a more general treatment, the reader can refer to [28].

## 6 OPTIMIZATION OF THE SYSTEM

This section condenses the previously found lumped parameters into a dynamic model. The impedance



representation is chosen in this example. The mobility approach with a current generator in place of a voltage generator leads to similar results.

## 6.1 Actuator dynamics

Constitutive equations are derived from the Euler-Lagrange equation using the Lagrangian defined by  $\mathcal{L} = \mathcal{T}_a - \mathcal{V}_a$  and the derivative of the dissipation function with respect to velocity. The generalized coordinates are the actuator displacement  $u_a$  and voltage  $v$ . The equations that govern this electromechanical system are:

$$M_a \ddot{u}_a(t) + B_a \dot{u}_a(t) + K_a u_a(t) = \gamma v(t) \quad (17)$$

$$C^S v(t) + \frac{1}{R} \int v(t) dt - \gamma u_a(t) = q(t); \quad (18)$$

where  $q$  is the electrical charge produced by the power supply. This set of constitutive equations models only the actuator. The impedance of the thin plate and the finger are added to complete the model of the entire device.

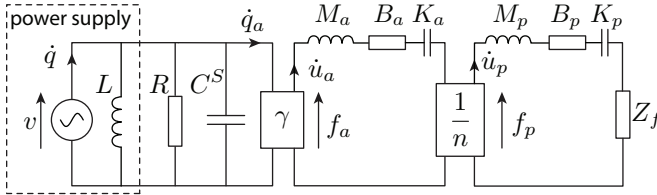


Fig. 6. Electromechanical model of the system. It includes a voltage generator and a parallel inductance  $L$  tuned to compensate the capacitor at the operating frequency.

To do so we can note that  $\dot{u}_p = n \cdot \dot{u}_a$  and  $f_p = \frac{1}{n} \cdot f_a$  so that the combined impedance of the plate and finger seen by the actuator is  $Z_p + Z_f = \frac{f_p}{\dot{u}_p} = \frac{1}{n^2} \frac{f_a}{\dot{u}_a}$  which leads to the equation

$$\gamma \frac{v}{\dot{u}_a} = Z_a + n^2 \cdot (Z_p + Z_f) \quad (19)$$

where  $Z_i = M_i j\omega + B_i + \frac{K_i}{j\omega}$ ,  $i = \{a, p\}$  are the impedances of the actuator and the plate respectively and  $Z_f$  is the impedance of the finger.

Considering the electrical side as well as the mechanical side and their interaction leads to the formulation pictured in Fig. 6. In an effort to reduce the load on the power supply, resonant devices often come with a added inductance. The inductance is tuned to cancel the capacitance at resonance:  $L = \frac{1}{\omega^2 C^S}$ . The electrical contribution of the inductor is incorporated into the impedance  $Z_e = (1/R + j(C^S \omega - 1/L\omega))^{-1}$ . The total impedance seen by the power supply is

$$Z_t = \frac{v}{\dot{q}} = \left( \frac{1}{Z_e} + \frac{\gamma^2}{Z_m + n^2 Z_f} \right)^{-1} \quad (20)$$

with  $Z_m = Z_a + n^2 \cdot Z_p$  the impedance of the plate and the actuator seen from the actuator side. Equation 20 captures the relationship between the current and the voltage at the electrical level. It depends on electrical as well as mechanical elements projected onto the electrical side.

## 6.2 Efficiency

In the present application, the efficiency  $\eta$  is defined by the ratio of the apparent power received by the finger  $P_o$  to the apparent electrical input power  $P_i$ . Apparent power captures the losses inherent to the system as well as the losses that an amplifier would have to bear if the load has a reactive component. The input power under harmonic excitation is  $P_i = |v \dot{q}| = |Z_t^{-1}| v^2$ . On the other hand, the power delivered to the finger is  $P_o = |Z_f| \dot{u}_p^2 = |Z_f \frac{\gamma^2 n^2}{(Z_m + n^2 Z_f)^2}| v^2$ . As the finger is modeled as a simple damper, it shows no reactive power and the apparent and real power are equal. The maximum of efficiency is found when the first derivative with respect to the load  $Z_f$  is zero:

$$\frac{d\eta}{dZ_f} = Z_e \gamma^2 \frac{Z_m^2 + \gamma^2 Z_e Z_m - (n^2 Z_f)^2}{(Z_m + n^2 Z_f)^2 (Z_m + n^2 Z_f + Z_e \gamma^2)^2} = 0 \quad (21)$$

Since the denominator is always finite, this leads to a condition on the circuit impedances for optimum electromechanical conversion:

$$Z_f = \frac{Z_m}{n^2} \sqrt{1 + \gamma^2 \frac{Z_e}{Z_m}} \quad (22)$$

The value of the optimum corresponds to a maximum of efficiency. Figure 7 shows a waterfall plot of the efficiency function for a given ratio between the electrical and mechanical impedances.

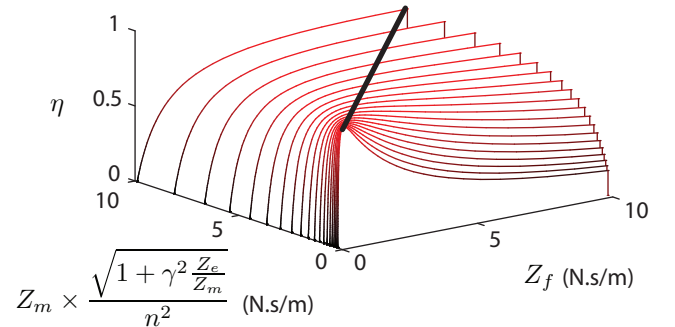


Fig. 7. Efficiency function for  $Z_e = 2000 \times Z_m$ ,  $n = 2$  and  $\gamma = .2$ . The diagonal line indicates the location of optimal efficiency.

The mechanical and electrical impedances,  $Z_m$  and  $Z_e$ , and amplification factor  $n$  and  $\gamma$  are functions of the thickness of both the actuator and the glass; therefore, the efficiency is also a function of both thicknesses. Figure 8 shows the efficiency for an set of devices which have a 100x90 mm workspace. The

presence of an inductor changes the location of the maximum of efficiency and increases its value. In addition, actuators made with hard piezoceramics exhibit higher efficiency than their soft piezoceramic counterparts.

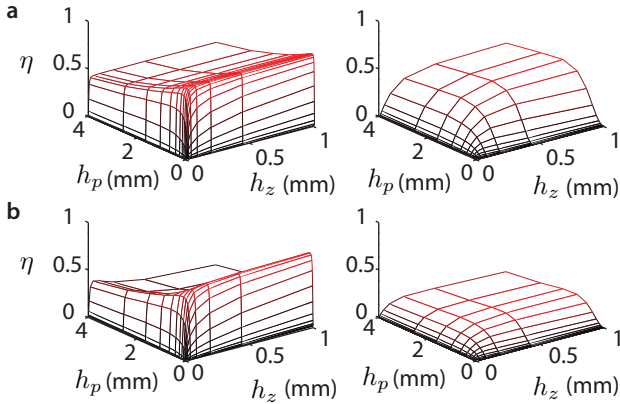


Fig. 8. Efficiency for piezoelectric actuators glued to a 120x90 mm glass ( $h_g = h_p$ ). Left column is with inductance and right column is without. **a.** Hard piezoceramic **b.** Soft piezoceramic.

### 6.3 Quality factor

The friction reduction device takes advantage of the resonance of the glass to achieve a large motion amplitude. To create complex friction waveforms, the carrier frequency corresponding to the normal mode being used is modulated in amplitude with the desired low frequency waveform. The more highly resonant the system is, the more time it will need to change amplitude. As a result, large quality (Q) factor will reduce the frequency bandwidth of the amplitude modulation of the resonant carrier wave. [17], [18]. For a carrier frequency of  $f_0 = 35$  kHz the Q factor that gives a modulation bandwidth of  $f_m = 500$  Hz is  $Q = f_0/2f_m = 35$ .

The Q factor is affected by both dissipation and storage elements. In order to achieve a low quality factor while providing a sufficient displacement of the plate, it is natural to minimize the storage elements such as the stiffness of the plate, and the capacitance of the piezoelectric actuator, while keeping the damping low. The quality factor is defined by the ratio of the maximum stored energy to the dissipated energy over a cycle multiplied by the frequency :  $Q = \omega \frac{U}{D}$ . For the schematic presented at Fig.6, the power dissipation is

$$D = (B_a + n^2(B_p + Z_f)) \dot{u}_a^2 + \frac{1}{R} v^2 \quad (23)$$

and the maximum energy stored at resonance is:

$$U = \frac{1}{2} \frac{K_a + n^2 K_p}{\omega^2} \dot{u}_a^2 + \frac{1}{2} C^s v^2 \quad (24)$$

In order to lower the quality factor, it is important to reduce the elastic storage in the plate by making

it thinner. The quality factor of the device is closely approximated by the quality factor of the glass with the finger. However as the actuator is made thinner and the glass has little dissipation, the electrical storage and dissipation are increasingly responsible for the quality factor. Figure 9 shows a simulation of the quality factor of the reference plate with a finger acting as a  $Z_f = 20$  N.s/m damper.

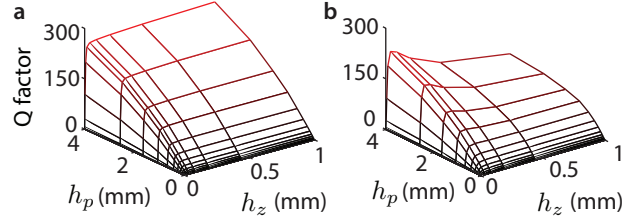


Fig. 9. Quality factor of an actuated plate with inductor and finger resting on it **a.** Hard piezoceramic **b.** Soft piezoceramic.

## 7 EXPERIMENTS

### 7.1 Ultrasonic plates

The model described in this paper has been validated with two resonating tactile plates. The first uses a thin 0.67 mm borosilicate glass substrate with a workspace of 60x20 mm<sup>2</sup> excited at 33 kHz. The piezoelectric actuators are 20x10 mm<sup>2</sup> wide by 0.55 mm thick, cut from a larger plate (SMPL21W21T05410, Steminc and Martins Inc, Miami, FL, USA). The second uses a 1.77 mm thick borosilicate substrate with a workspace of 100 mm by 52 mm on to which 0.7 mm thick hard piezoelectric actuators (SMPL26W16T07111, Steminc and Martins Inc, Miami, FL, USA) are glued. The resonance is calculated to be close to 33 kHz and 30 kHz for the small and large plate respectively. The piezoelectric actuators are bonded to each side of the glass using epoxy (Hysol E-30CL, Hankel AG, Dusseldorf, Germany). The material properties of hard and soft piezoelectric materials used in this article are reported Table 1. Picture 10a shows both devices covered with salt while excited at their resonant frequencies. The salt, trapped at the location of nodal lines, reveals Chladni patterns.

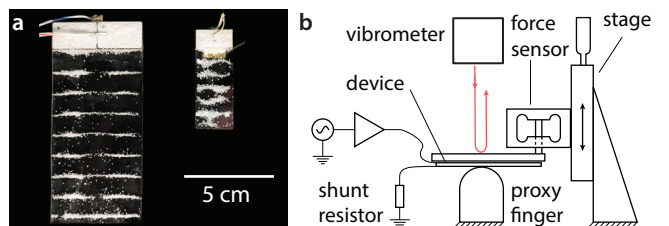


Fig. 10. **a** Tactile plates used in the experiments **b** Experimental setup.



## 7.2 Material and methods

Figure 10b illustrates the experimental setup. The ultrasonic plate was mounted to an acrylic frame via 1 mm thick foam tape attached to the extremities of 4 nodal lines. This unobtrusive mounting provided a free boundary condition for each edge of the plate. The amplitude of the vibration was monitored during mounting to ensure that the boundary conditions did not influence the resonant frequency or the quality factor. The displacement of the glass and the actuator were measured using a scanning laser Doppler vibrometer (PSV-400, Polytec GmbH, Waldbronn, Germany) which has a noise floor of 10  $\mu\text{m/s}$ . At the same time, the current was evaluated by a 100  $\Omega \pm 0.1\%$  resistor placed in series with the piezoelectric actuator. The noise from the current measurement remained below 3  $\mu\text{A}$ . The actuator was driven with a 20x high-voltage amplifier (A-303, A. A. Lab System LTD, Ramat-Gan, Israel), able to provide  $\pm 100\text{ V}$  up to 100 kHz. Signals were generated and acquired using a 16-bit digital acquisition board at 250 kHz sampling rate (USB-6361, National Instruments Corp., Austin, TX, USA). The excitation signal was a one second swept-sine  $\pm 3\text{ kHz}$  around the resonance of the device. To avoid any artifacts due to quantization and finite sampling rate, the excitation signal was filtered with a 10 kHz low-pass reconstruction filter. The amplifier used in these experiments was optimized for strictly capacitive loads, therefore no inductor was used.

## 7.3 Results

### 7.3.1 Mode shape and frequency response

The acoustic and electrical measurements of both devices are in good agreement with the values predicted by the model. Figure 11a shows the frequency response of the device around the working frequency. The second order model proposed in this article fits the frequency around a bandwidth of  $\pm 1\text{ kHz}$ . As expected, it fails to describe other resonances of the device that appear further away from the normal mode for which the plate is designed. The plate stiffness  $K_p$  was modified to account for the slight discrepancy between the designed and the effective resonance frequency. The amplification factor  $n$  was adjusted to the actual measured value. In each case, the fitted value was within 10% of the value predicted based on the dimensions and material properties. The electrical impedance around the working frequency also shows good agreement with the model predictions. Figure 11b shows the impedance from measurements and model. The discrepancies are likely to be due to non-linearities in the loss mechanism of piezoelectric ceramic [27]. The spatial features of the model are also well captured. Figure 11c shows the measured amplitude of the glass and actuator at the working frequency. The glass plate follows the mode shape

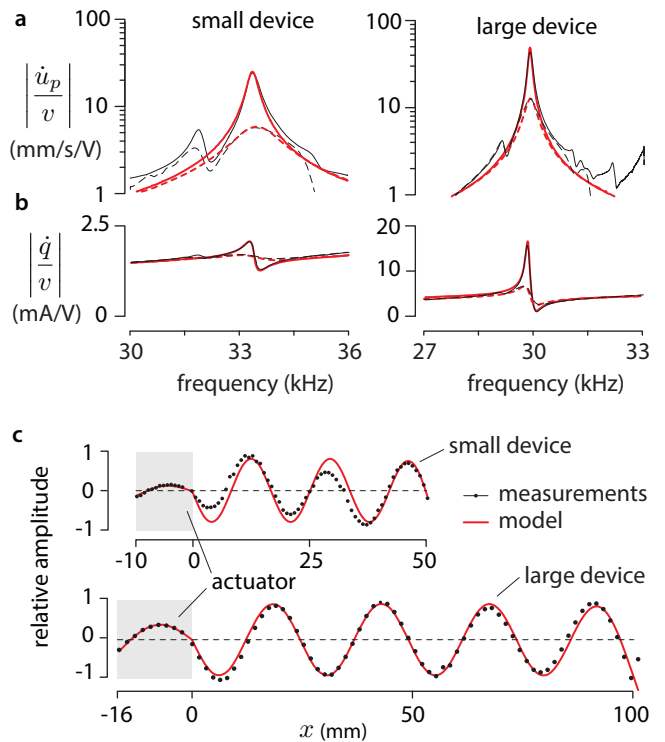


Fig. 11. Frequency response and mode shape of both devices. The plain lines represent the unloaded condition and the dashed lines illustrate the response when a finger is pressing with 0.1 N and 1 N for the small and large devices respectively. The actual mode shape of the plate deviates from the theory of a simple plate model with pinned-free boundary condition. This discrepancy is due to the complex interaction at the interface between the plate and the actuator.

of a pinned-free plate and the actuator a free-pinned plate with high precision. Higher order behavior is introduced due to the non-trivial interaction at the boundary between the actuator and the plate. The measurement shows an unambiguous amplification of the amplitude of motion between the glass and the actuator.

### 7.3.2 Power efficiency

The efficiency of each device is measured from the ratio between the electromechanical admittance squared to the electrical admittance multiplied by the added damping  $Z_f$ ,  $\eta = |Z_f| \left( \frac{\dot{u}_p}{v} \right)^2 \left| \frac{\dot{q}}{v} \right|^{-1}$  which follows the same definition as in section 6.2. The variation of the external load is achieved by pressing the device against a proxy fingertip made of a 15 mm-radius hemisphere in silicone (Ecoflex 00-10, NuSil Technology, Carpinteria, CA, USA). This material is known to mimic the mechanical behavior of soft tissue and its adhesive properties ensure a proper bonding [29]. The center of the proxy finger was placed on an anti-node where the plate provides a maximum of

deformation to the external load. Swept-sine excitation was provided to the amplifier and the both the current and vibration amplitude frequency responses were recorded. The added impedance is found by the change in amplitude and resonant frequency of the system. The resonant frequency did not significantly change as the added mass and stiffness of the proxy were small with respect to both devices. The added impedance was treated as a pure damper.

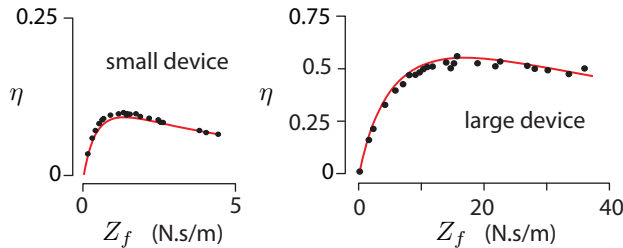


Fig. 12. Efficiency of both devices. Circles represent the measurement points and the line the prediction of the model.

A comparison between observed and predicted efficiencies is shown in Figure 12. The model shows a good agreement with experimental data for both devices. The large device exhibits higher efficiency for two main reasons. First, the impedance of the device has a magnitude similar to that of the fingertip. This reduces the impact of the additional damping on the amplitude of the motion and the power output. Second, the hard piezoelectric used in the actuators of the larger device also contribute to higher efficiency. The low-loss material enables large displacements while keeping the electrical consumption low.

### 7.3.3 Fingert impedance

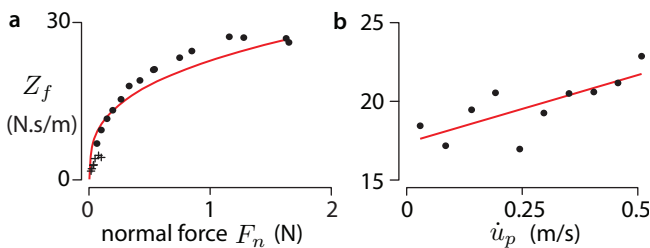


Fig. 13. Evolution of the impedance provided by a fingertip. The data from the larger device are represented by dots and by crosses for the smaller device. Lines show regressions. **a.** With respect to the normal force. **b.** With respect to increasing amplitude of stimulation for a normal force of 0.5 N.

The estimate of finger impedance derived in section 3.1 is based on measurement of the skin made in quasi-static and low frequency conditions. The behavior at higher frequency includes complex dynamics due in part to the phenomenon of friction reduction. During the interaction with an plate excited

with transverse waves, the contact between a plate and the fingertip can be broken thus reducing the friction force. This behavior is likely to introduce an additional dissipation mechanism as the elastic energy stored into the skin while in contact is dissipated during the breakaway. While a complete understanding is beyond the scope of this article, an estimate of the impedance provided by a finger is of value for the optimization procedure. The estimates are made with the lead author's fingertip. In order to measure the fingertip damping, we analyzed the added impedance provided by the skin pressed into contact with the small and large device. The knowledge of dynamic parameters of each plate and the real time measurement of the amplitude of motion allows for the recovery of the added impedance. As for the proxy finger, the change in resonant frequency was not significant since the added mass is an order of magnitude smaller than the mass of either plate. The precise value of the reactive part of the impedance is not reported as the uncertainty is likely to be higher than the measurement. The maximum frequency shift produced by the fingertip on the large device was about -160 Hz which translated to 0.4 g of additional mass. A force sensor (LSM250, Futek AST Inc. Irvine, CA, USA) records the pressing force applied by the fingertip. The results for a normal force varying from 0 to 1.6 N under a 2 V excitation are shown figure 13a.

In the low frequency range, the impedance of the fingertip is known to increase with normal force. The reason behind this increase is that the spherical shape of the finger causes the contact surface to increase with increasing normal load [30]. A large area of contact will engage more tissue, thus increasing the dissipation of vibration. A power-law regression shows that  $Z_f \approx 24 \times F_n^{0.3}$ .




Figure 13b shows the dependency of the finger impedance on amplitude of stimulation, when pressing at 0.5 N. While most of the damping is present for small motion, its value increases with the amplitude of the vibration. This is likely to be caused by the mechanical losses due to the breakaway between the plate and the fingertip that are involved in the friction reduction mechanism [31]. The linear regression gives an intercept at 16 N.s/m and a slope of 2.8 (N.s/m)/(m/s)

## 8 DISCUSSION

### 8.1 Scaling law

Ultrasonic surface-haptic devices modulate friction with the finger via the interaction with a standing wave. The finger dissipates the acoustic energy stored in the glass and therefore the minimum energy consumption has to be in the order of 1 W, as found from measurements reported in section 7.3.3. Further energy dissipation mechanisms arise from the glass and piezo-electric material. Naturally, the larger the

TABLE 2  
Mode shape and lineic parameters of the actuator for various boundary conditions.

				
mode shape	$s(x)$	$\sin(\beta_0 x)$	$\sin(\beta_0 x) - \frac{\sin(\beta_0 l)}{\sinh(\beta_0 l)} \sinh(\beta_0 x)$	$\sin(\beta_0 x) + \frac{\sin(\beta_0 l)}{\sinh(\beta_0 l)} \sinh(\beta_0 x)$
	$\beta_0 l$	$\pi$	$\approx 3.927$	$\approx 3.927$
mean square shape	$\int_0^l s^2(x) dx$	$l/2$	$l/2$	$l/2$
mean square curv.	$\int_0^l \left(\frac{d^2 s}{dx^2}\right)^2 dx$	$\beta_0^4 \frac{l}{2} = \pi^4/2l^3$	$\beta_0^4 \frac{l}{2}$	$\beta_0^4 \frac{l}{2}$
average curvature	$\int_0^l \frac{d^2 s}{dx^2} dx$	$-\beta_0^2 \frac{2l}{\pi} = -2\pi/l$	$\approx -0.26 \beta_0^2 l$	$\approx -0.61 \beta_0^2 l$

interface, the higher the losses. The additional losses grow in proportion to the workspace area. For a screen with a 16:9 aspect ratio built from 1 mm-thick glass and actuated by 0.5 mm-thick piezoceramic glued along the width, the dissipation at 35 kHz grows at a rate of 20 W per m<sup>2</sup>.

## 8.2 Piezoelectric material choice

Soft piezoelectric materials usually present a force factor  $\gamma$  which is  $\approx 25\%$  higher than their *hard* counterparts. This gain is overshadowed by the both the electrical and mechanical dissipation of the soft material that can reach 50 times the dissipation of hard piezoceramic. The final amplitude experienced by the finger is related to the ratio of the damping  $B_a$  and the force factor  $\gamma$  which clearly gives an advantage to the *hard* material when efficiency is critical. However the designer of surface haptic a device might want to optimize the display for a low Q factor while keeping a large amplitude of deformation, in the case where efficiency is secondary and the rate of change of the amplitude of the ultrasonic wave –for texture reproduction for instance– is the main design factor [18]. In this case, a soft ceramic might be preferred.

## 8.3 Conclusion

This paper presents a comprehensive model of the electro-mechanical behavior of a rectangular plate excited by piezoelectric actuators. This configuration is central in the development of devices that modify the friction with a bare fingertip in real time and thus are able to render complex tactile sensations on a 2d plane. The model converts the acoustic behavior into lumped elements that capture the behavior of the plate, actuator and fingertip close to the working frequency. The simplicity of the lumped-parameter model allows for optimal design of the device with respect to efficiency or quality factor. Performance assessment of two borosilicate glass plates equipped with hard and soft piezoelectric actuators shows that the model predictions are in good agreement with experiment.

The efficiency of the device is determined by the values of both mechanical and the electrical impedances with respect to the impedance of the finger. This study shows that, for a given finger impedance, there exists an optimal configuration of electromechanical parameters that maximize the ratio between the mechanical power output to the finger and the electrical power input to the system. This optimum corresponds to a configuration in which the piezoelectric actuator is small enough to dissipate less energy but large enough to provide the necessary force for deforming the fingertip. In general the use of hard piezoelectric material and an inductor on the power supply helps to increase efficiency. The low dissipation and high quality factor of the system that are required for high efficiency do not, however, favor fast amplitude modulation, and therefore the bandwidth of the tactile waveforms that can be reproduced. Lastly, this model is purely linear and does not take into account non-linearities arising from the electric field saturation which create more losses and disfavor even more thinner piezoelectric actuators.

In conclusion, this paper presents a model of a typical device configuration and its efficiency optimization. The biomechanics of the fingertip and their implications for optimization have also been treated. The findings presented here are likely to be of interest to designers of surface-haptic devices.

## ACKNOWLEDGMENTS

The authors would like to thank Prof. Thomas Royston of the University of Illinois Chicago for the use of the vibrometer. They are also grateful for the anonymous reviews that helped improved the clarity of the article. This work has been supported by National Science Foundation under grants IIS-0964075 and IIS-1302422.

## APPENDIX A INFLUENCE OF BOUNDARY CONDITIONS

The attachment of the actuator will determine its mode shape and consequently its length, dynamic

parameters and electromechanical conversion factor. The mode shape is linked to these parameters by the integrals of the shapes and their derivatives with respect to the actuator length. Table 2 shows the value of each integral for simply-supported, clamped and free boundary conditions. The connection of the actuator with the plate is made at a nodal point. Therefore, the other boundary is modeled as simply supported.

## REFERENCES

- [1] I. Poupyrev and S. Maruyama, "Tactile interfaces for small touch screens," in *Proceedings of the 16th annual ACM symposium on User interface software and technology*, 2003, pp. 217–220.
- [2] H.-Y. Yao and V. Hayward, "Design and analysis of a recoil-type vibrotactile transducer," *The Journal of the Acoustical Society of America*, vol. 128, p. 619, 2010.
- [3] J. M. Romano and K. J. Kuchenbecker, "Creating realistic virtual textures from contact acceleration data," *IEEE Transactions on Haptics*, vol. 5, no. 2, pp. 109–119, 2012.
- [4] S.-Y. Kim and J. C. Kim, "Vibrotactile rendering for a traveling vibrotactile wave based on a haptic processor," *IEEE Transactions on Haptics*, vol. 5, no. 1, pp. 14–20, 2012.
- [5] C. Hudin, J. Lozada, M. Wiertelowski, and V. Hayward, "Trade-offs in the application of time-reversed acoustics to tactile stimulation," in *Proceedings of Eurohaptics 2012, LNCS 7283, Part I*, 2012, pp. 218–226.
- [6] C. Hudin, J. Lozada, and V. Hayward, "Localized tactile stimulation by time-reversal of flexural waves: Case study with a thin sheet of glass," *Proceedings of IEEE World Haptics Conference (WHC)*, pp. 67–72, 2013.
- [7] R. M. Strong and D. Troxel, "An electrotactile display," *IEEE Transactions on Man-Machine Systems*, vol. 11, no. 1, pp. 72–79, 1970.
- [8] O. Bau, I. Poupyrev, A. Israr, and C. Harrison, "Teslatouch: electrovibration for touch surfaces," in *Proceedings of the 23rd annual ACM symposium on User interface software and technology*, 2010, pp. 283–292.
- [9] D. J. Meyer, M. A. Peshkin, and J. E. Colgate, "Fingertip friction modulation due to electrostatic attraction," in *Proceedings of IEEE World Haptics Conference (WHC)*, 2013, pp. 43–48.
- [10] T. Watanabe and S. Fukui, "A method for controlling tactile sensation of surface roughness using ultrasonic vibration," in *Proceedings of IEEE International Conference on Robotics and Automation*, vol. 1, 1995, pp. 1134–1139.
- [11] M. Biet, F. Giraud, and B. Lemaire-Semail, "Squeeze film effect for the design of an ultrasonic tactile plate," *IEEE Transactions on Ultrasonics, Ferroelectrics and Frequency Control*, vol. 54, no. 12, pp. 2678–2688, 2007.
- [12] L. Winfield, J. Glassmire, J. E. Colgate, and M. Peshkin, "T-pad: Tactile pattern display through variable friction reduction," in *Proceedings of World Haptics Conference (WHC)*, 2007, pp. 421–426.
- [13] N. D. Marchuk, J. E. Colgate, and M. A. Peshkin, "Friction measurements on a large area tpad," in *Proceedings of IEEE Haptics Symposium*, 2010, pp. 317–320.
- [14] F. Giraud, M. Amberg, B. Lemaire-Semail, and G. Casiez, "Design of a transparent tactile stimulator," in *Proceedings of IEEE Haptics Symposium*, 2012, pp. 485–489.
- [15] K. J. Son, M. Kim, and K. Kim, "Analytical modeling of disk-type piezoelectric variable friction tactile displays," in *Proceedings IEEE/ASME International Conference on Advanced Intelligent Mechatronics*, 2013, pp. 1725–1730.
- [16] F. Giraud, M. Amberg, R. Vanbelleghem, and B. Lemaire-Semail, "Power consumption reduction of a controlled friction tactile plate," in *Proceedings of Eurohaptics 2012, LNCS 6192, Part II*. Springer, 2010, pp. 44–49.
- [17] F. Giraud, M. Amberg, and B. Lemaire-Semail, "Design and control of a haptic knob," *Sensors and Actuators A: Physical*, vol. 196, pp. 78–85, 2013.
- [18] D. J. Meyer, M. Wiertelowski, M. Peshkin, and J. E. Colgate, "Dynamics of ultrasonic and electrostatic friction modulation for rendering texture on haptic surfaces," in *Proceedings of IEEE Haptics Symposium*, 2014, pp. 218–226.
- [19] E. Dimitriadis, C. Fuller, and C. Rogers, "Piezoelectric actuators for distributed vibration excitation of thin plates," *Journal of Vibration and Acoustics*, vol. 113, no. 1, pp. 100–107, 1991.
- [20] Q. Wang and V. Hayward, "In vivo biomechanics of the fingerpad skin under local tangential traction," *Journal of biomechanics*, vol. 40, no. 4, pp. 851–860, 2007.
- [21] E. R. Serina, E. Mockensturm, C. Mote Jr, and D. Rempel, "A structural model of the forced compression of the fingertip pulp," *Journal of biomechanics*, vol. 31, no. 7, pp. 639–646, 1998.
- [22] C. Wallace, "Radiation resistance of a rectangular panel," *The Journal of the Acoustical Society of America*, vol. 51, p. 946, 1972.
- [23] K. Graff, *Wave Motion in Elastic Solids*. Dover Publications, 1975.
- [24] A. Preumont, *Mechatronics: dynamics of electromechanical and piezoelectric systems*. Springer, 2006, vol. 136.
- [25] R. Holland, "Representation of dielectric, elastic, and piezoelectric losses by complex coefficients," *IEEE Transactions on Sonics and Ultrasonics*, vol. 14, no. 1, pp. 18–20, 1967.
- [26] J. D. Larson III, P. Bradley, S. Wartenberg, and R. C. Ruby, "Modified butterworth-van dyke circuit for fbar resonators and automated measurement system," in *IEEE Ultrasonics Symposium*, vol. 1, 2000, pp. 863–868.
- [27] K. Uchino and S. Hirose, "Loss mechanisms in piezoelectrics: how to measure different losses separately," *IEEE Transactions on Ultrasonics, Ferroelectrics and Frequency Control*, vol. 48, no. 1, pp. 307–321, 2001.
- [28] A. D. Nashif and J. P. Henderson, *Vibration damping*. John Wiley & Sons, 1985.
- [29] T. J. Royston, Z. Dai, R. Chaunsali, Y. Liu, Y. Peng, and R. L. Magin, "Estimating material viscoelastic properties based on surface wave measurements: A comparison of techniques and modeling assumptions," *The Journal of the Acoustical Society of America*, vol. 130, no. 6, p. 4126, 2011.
- [30] M. Wiertelowski and V. Hayward, "Mechanical behavior of the fingertip in the range of frequencies and displacements relevant to touch," *Journal of biomechanics*, vol. 45, no. 11, pp. 1869–1874, 2012.
- [31] X. Dai, J. E. Colgate, and M. A. Peshkin, "Lateralpad: A surface-haptic device that produces lateral forces on a bare finger," in *Proceedings of IEEE Haptics Symposium*, 2012, pp. 7–14.



**Michaël Wiertelowski** earned his PhD degree at the Université Pierre et Marie Curie under the auspices of the Laboratoire d'Intégration des Systèmes et des Technologies of the Commissariat à l'Énergie Atomique (CEA-IST) in France. His doctoral thesis has received the 2012 Eurohaptics Society Thesis Award. He is now postdoctoral researcher at Northwestern University.



**J. Edward Colgate** received the PhD degree from MIT in 1988 and is the Breed University Professor of Design at Northwestern University in Evanston, Illinois. He was the founding Editor-in-Chief of the IEEE Transactions on Haptics. His research interests are in human-machine interaction, especially haptic interface. He is a Fellow of the IEEE.